Supplementary Information

Design, synthesis, conformational analysis and nucleic acid hybridisation properties of thymidyl pyrrolidine-amide oligonucleotide mimics (POM).

Hickman *et al.*

ESI Table 1. The standard enthalpies of formation, phase angle (P), cyclic torsion angles $\nu_0 \rightarrow \nu_4$, and the torsion angle C3´-C4´-N1-C2 (χ) for the conformers **A**-**D** in figure 3. The structure of the lowest energy *trans*-conformers **A** and **B** are shown in figure 4 of the main text.

ESI Figure 1. Numbering system for ^{1}H NMR assignment of T_2-POM.3HCl **30.**

ESI Table 2a &b. ^{1}H NMR chemical shifts (δ_H) and coupling constants (J_{HH}) for T_2-POM.3HCl **30.**

ESI Table 3. ROE cross peaks observed in the ROESY spectrum of T_2-POM.3HCl **30.**

ESI Figure 2. Regions of the ^{13}C spectra of Phth-T_n-Boc (n = 2→4) **21**, **32** and **33** run in CD_3OD at 100 MHz. Spectra **a-c** show the thymine *C*H_3 peaks in the region at *ca*. 11-12 ppm. Spectra **d-f** show the thymine C4 carbon peaks in the region at *ca*. 166-167 ppm.

ESI Figure 3. Sections of the ^{1}H NMR spectra of **(a)** Phth-T_5-Boc-POM **34** and **(b)** Phth-T_4-Boc-POM **33**, run in DMSO-d_6 showing five and four thymine NH protons, respectively.

ESI Figure 4. Analytical HPLC trace of Phth-T_5-POM **35**. 5HCl run under the following conditions: Hypersil Elite C-18, 3 μ, 150 x 4.6 mm column; Solvent A 50mM tris buffer at pH 7.8; Solvent B acetonitrile; The flow rate was 1 mLmin^{-1} with a gradient elution of 20% B increasing to 50% B over 30 min.

ESI Figure 5. Electrospray ionisation (ESI) mass spectrum of Phth-T_5-POM **35**.

ESI Figure 6. Variation of absorption (A_{260}) with temperature curves for an equimolar mixture of Phth-T_5-POM **35** and poly(rA) (42 μM each in bases) in buffer A (10 mM K_2HPO_4) adjusted to 120 mM K^+, pH 7.0 for a typical cycle of fast heating (5 ˚C/min), slow cooling (0.2 ˚C/min)

and slow heating (0.2 ˚C/min). The large hysteresis between the slow heating and slow cooling curves indicates that the rate of association and dissociation is less than the rate of heating and cooling such that equilibrium between **35** and poly(rA) is not attained. Typically at a heating/cooling rate of 0.2 ˚C/min little or no hysteresis is observed for native duplex forming oligonucleotides, suggesting that **35** and poly(rA) associate and dissociate slowly compared with the hybridisation of native nucleic acids. This cycle of heating/cooling was used for determining T_ms except where stated otherwise.

ESI Figure 7. UV melting curves for T_5-POM **3** and poly(rA) (42 μM each in bases) in buffer A (120 mM K^+, pH 7.0) following fast heating (5 ˚C/min) then cooling and heating at different rates of: 5.0 (Δ), 2.0 (□), 1.0 (●), 0.5 (▲) and 0.1(■) ˚C/min). The larger hyperchromic shifts at slower rates of heating/cooling are presumably a consequence of the greater extent of duplex association and dissociation during the cooling and heating cycles respectively.

ESI Figure 8. Plot of T_m *vs* rate of heating/cooling (from ESI figure 7). This shows that the observed T_m for Phth-T_5-POM **35** and poly(rA) (120 mM K^+, pH 7.0) is higher at lower rates of heating/cooling. By extrapolating to an infinitely slow rate of heating/cooling the true equilibrium T_m was determined to be *ca*. 49 ˚C.

ESI Figure 9. UV thermal denaturation curves of Phth-T_5-POM **35** and poly(rA) (42 μM each in bases, buffer A, pH 7.0) at different ionic strengths: 0.12 (●), 0.22 (■), 0.62 (▲) and 1.20 (○) M K^+. An increase in ionic strength is accompanied by a moderate increase in T_m. The lower hyperchromic shifts observed at higher ionic strength are probably due to slower rates of association/dissociation of **35** with Poly(rA).

ESI Figure 10. UV thermal denaturation curves of Phth-T_5-POM **35** and poly(rA) (42 μM each in bases, buffer A, 0.12 M K^+) at different pHs: 6.0 (■), 6.5 (●), 7.0 (▲), 7.5 (□) and 8.0 (○). Considerably higher T_m values and larger hyperchromic shifts are observed at lower pH. The later is a reflection of faster association at lower pH such that during the annealing cycle a higher proportion of strands have hybridised.

ESI Figure 11. Variation of A_{260} with time immediately upon mixing an equimolar (42 μM each in bases) amount of either Phth-T_5-POM **35** (▲) or Lys-T_5-LysNH_2-PNA (Δ) with Poly(rA) in buffer A adjusted to 0.12 M K^+ and pH 7.0 at 25 ˚C.

ESI Figure 12.Variation of A_{260} with time immediately upon mixing equimolar Phth-T_5-POM **35** and Poly(rA) (42 μM each in bases) in buffer A adjusted to pH 7.0 at 25 ˚C with change in ionic strengths: 0.62 (●), 0.22 (▲), 0.12 (□) and 0.02 (○) M K^+.

ESI Figure 13. Variation of A_{260} with time immediately upon mixing equimolar Phth-T_5-POM **35** and Poly(rA) (42 μM each in bases) in buffer A adjusted to 0.12 M K^+ at 25 ˚C with change in pH: 8.0 (■), 7.0 (●), 6.0 (▲).

ESI Figure 14. Sensogram of response (*RU*) *vs.* time upon injecting Phth-T_5-POM **35** at 80 μM over flow cell (Fc) 2 derivatised with 5´-biotin-$d(A)_{20}$ and Fc 3 derivatised with 5´-biotin-$r(A)_{20}$ for 300 sec. In buffer A adjusted to 0.12 M K^+ or 1.2 M K^+ and pH 7.0. After 300 s, buffer alone was passed over the surfaces to enable Phth-T_5-POM to dissociate. All sensograms are corrected for Phth-T_5-POM binding to the underivatised dextran surface (Fc 1). [0.12 M K^+, $r(A)_{20}$ (■); 0.12 M K^+, $d(A)_{20}$ (●); 1.20 M K^+, $r(A)_{20}$ (□); 1.20 M K^+, $d(A)_{20}$ (○)]

ESI Figure 15. Sensogram of response *vs* time upon injecting Phth-T_5-POM **35** at 80 μM over Fc 1-4 [$r(A)_{20}$ (■); $d(A)_{20}$ (●); *NFκB* (▲); underivitised (Δ)] for 300 s in buffer A adjusted to 0.12 M K^+ and pH 6.0. After 300 s, buffer alone was passed over all the surfaces for a further 300 s.

ESI Figure 16. Sensogram of response *vs* time upon injecting Phth-T_5-POM **35** at 80 μM over Fc 1-4 [$d(A)_{20}$ (●); $r(A)_{20}$ (■); *NFκB* (▲); underivitised (Δ)] for 300 s in buffer A adjusted to 0.12 M K+ and pH 5.0. After 300 s, buffer alone was passed over all of the surfaces.

Conformers	Torsion angles / degrees							ΔH^o /
	ν_0	ν_1	ν_2	ν_3	ν_4	χ	P	(*kcal/mol*)
A	–20.82	–3.86	27.97	–40.20	36.84	–166.97	48	93.97
B	4.34	19.96	–37.49	40.29	–27.10	–125.83	198	94.54
C	–14.64	–10.64	32.59	–41.12	33.76	–165.65	38	97.68
D	4.34	19.96	–37.49	40.29	–27.10	–126.22	198	95.15

Table 1

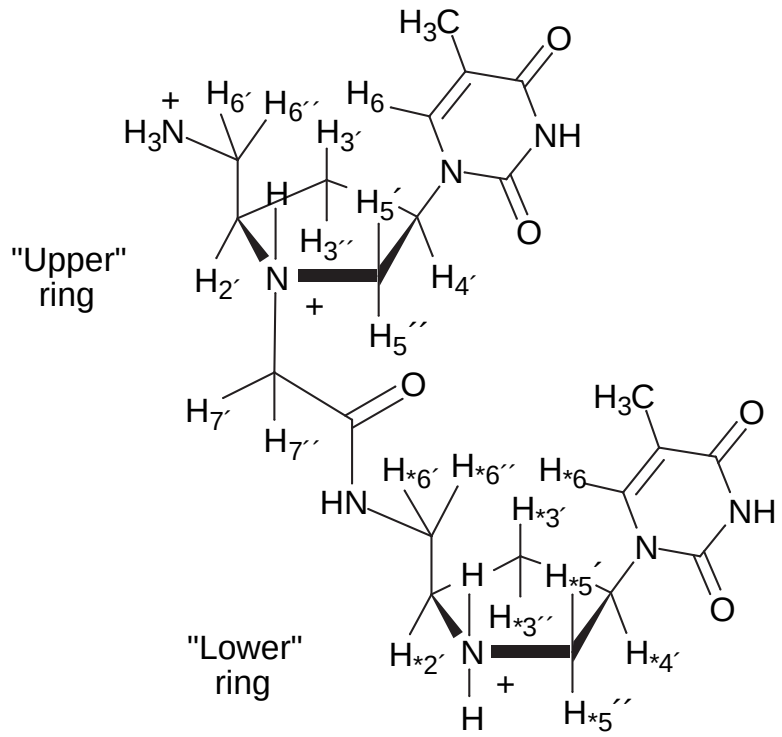

T_2-POM (**30**)

ESI Figure 1.

Table 2 (a)

Upper			Lower		
3.38 (6′)	Σ	21.3	3.86 (*6′)	Σ	19.4
	J 6′-6′′	13.4		*J* 6′-6′′	15.3
	J 6′-2′	7.8		*J* 6′-2′	4.1
3.51 (6′′)	Σ	17.2	3.86 (*6′′)	Σ	19.4
	J 6′-6′′	13.7		*J* 6′-6′′	15.3
	J 6′′-2′	3.4		*J* 6′′-2′	4.1
3.69 (2′)		obscured	3.93 (*2′)	Σ	29.7
2.19 (3′)	Σ	30.4	2.26 (*3′)	Σ	32.2
	J 3′-3′′	14.0		*J* 3′-3′′	14.3
	J	9.9		*J*	11.1
	J	6.2		*J*	6.5
2.93 (3′′)	Σ	31.0	2.77 (*3′′)	Σ	31.6
	J 3′-3′′	13.9		*J* 3′-3′′	14.3
	J	9.6		*J*	9.6
	J	7.4		*J*	7.4
5.03 (4′)	Σ	27.5	4.86 (*4′)	Σ	28.4
3.91 (5′)	Σ	16.3	3.81 (*5′)	Σ	16.3
	J 5′-5′′	12.5		*J* 5′-5′′	13.4
	J 4′- 5′	3.7		*J* 4′- 5′	2.8
3.47 (5′′) (e′′)	Σ	21.2	3.70 (*5′′)	Σ	21.2
	J 5′-5′′	12.5		*J* 5′-5′′	13.4
	J 4′- 5′′	8.8		*J* 4′- 5′′	7.8
3.79 (7′) (x′)	*J* 7′-7′′	16.1			
4.11 (7′′) (x′′)	*J* 7′-7′′	16.1			

Table 2 (b)

δ_H	2′	3′	3′′	4′	5′	5′′	6′	6′′	7′	7′′	6	CH_3
Upper	3.69	2.19	2.93	5.03	3.91	3.47	3.38	3.51	3.79	4.11	7.61	1.88
Lower	3.93.	2.26	2.77	4.86	3.81	3.70	3.86	3.86	----	----	7.48	2.00

J_{HH}	2′-3′ (b-c′)	2′-3′′ (b-c′′)	2′-6′ (b-a′)	2′-6′′ (b-a′′)	3′-3′′ (c′-c′′)	3′-4′ (c′-d′)	3′′-4′ (c′′-d′)	4′-5′ (d′-e′)	4′-5′′ (d′-e′′)	5′-5′′ (e′-e′′)	6′-6′′ (a′-a′′)	7′-7′′ (x-x′′)
Upper	9.9	7.4	7.8	3.4	14.0	6.2[†]	9.6[†]	3.7	8.8	12.5	13.6	16.1
Lower	11.1	7.4[$]	4.1	4.1	14.3	6.5[$]	9.6[$]	2.8	7.8	13.4	15.3	----

†-Σ4′= 27.5 and *J* 4′-5′ + *J* 4′-5′′ = 12.5. Therefore *J* 4′-3′ + *J* 4′-3′′ = 15 which is most consistent with *J* 4′-3′ = 6.2 and *J* 4′-3′′ = 9.6. Thus *J* 2′-3′ and *J* 2′-3′ can also be derived. [$] similar arguments that depend on the observed Σ2′ and Σ4′, for the lower ring also lead to the assignment of coupling constants as shown.

Table 3

Upper			Lower		
ROE (strong)	ROE (weak)	NO ROE	ROE (strong)	ROE (weak)	NO ROE
5´´-4´		5´-4´	*5´-*4´		
5´-6		5´-6	*5´´-*4´		
6- 4´			*5´-*6		*5´-*6
6- 3´		6- 3´´	*6-*4´		
3´´-2´		3´-2´	*6-*3´		*6-*3´´
2´-6´	3´´-6´		*3´´-*2´		*3´-*2´
	3´-6´´	3´´-6´´		*3´´-*6´/6´´	
4´-3´´	4´-3´		*4´-*3´´	*4–*3´ (v.v. weak)	
6´-7´´			*3´-*6´/6´´		
6´´-7´´			*3´–*5´´		
	2´-7´´				*7´-*6´/6´´
5´´-7´		5´-7´/7´´			*7´´-*6´/6´´
		2´-6 ´			
		2´-6´´			(no ROEs - between rings)

The two spin systems of the top and bottom pyrrolidine rings were assigned by TOCSY and DQF-COSY experiments. Protons of the top ring are clearly distinquished by noticeable ROEs (7´´-6´, 7´´-6´´ and 7´-5´´) to the isolated spin system 7/7´´. ROEs between 7/7´´ and protons on the lower ring are absent. Strong ROEs were present between 5´´- 4´ and 3´´-2´, were used to distinquish the diasterotopic protons H3´ /H3´´ and H5´/H5´´ . In contrast ROEs 5´- 4´ and 3´-2´ are clearly absent. Spectra are available upon request. Note grey areas in ROESY spectra are negative peaks due to TOCSY breakthrough, particularly when there is strong geminal coupling.

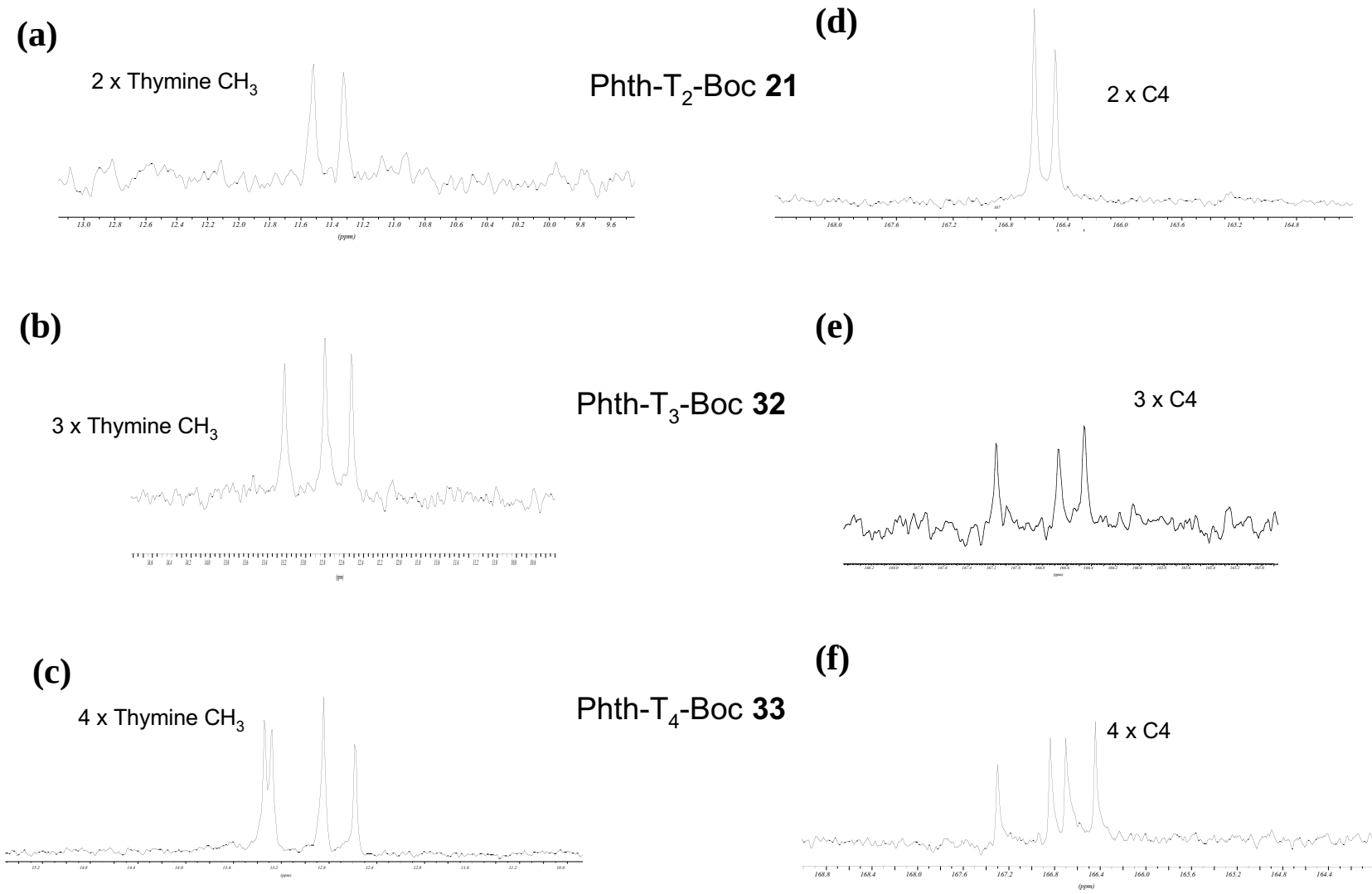
(a)
2 x Thymine CH3
Phth-T2-Boc 21
(d)
2 x C4
(b)
3 x Thymine CH3
Phth-T3-Boc 32
(e)
3 x C4
(c)
4 x Thymine CH3
Phth-T4-Boc 33
(f)
4 x C4

Figure 2

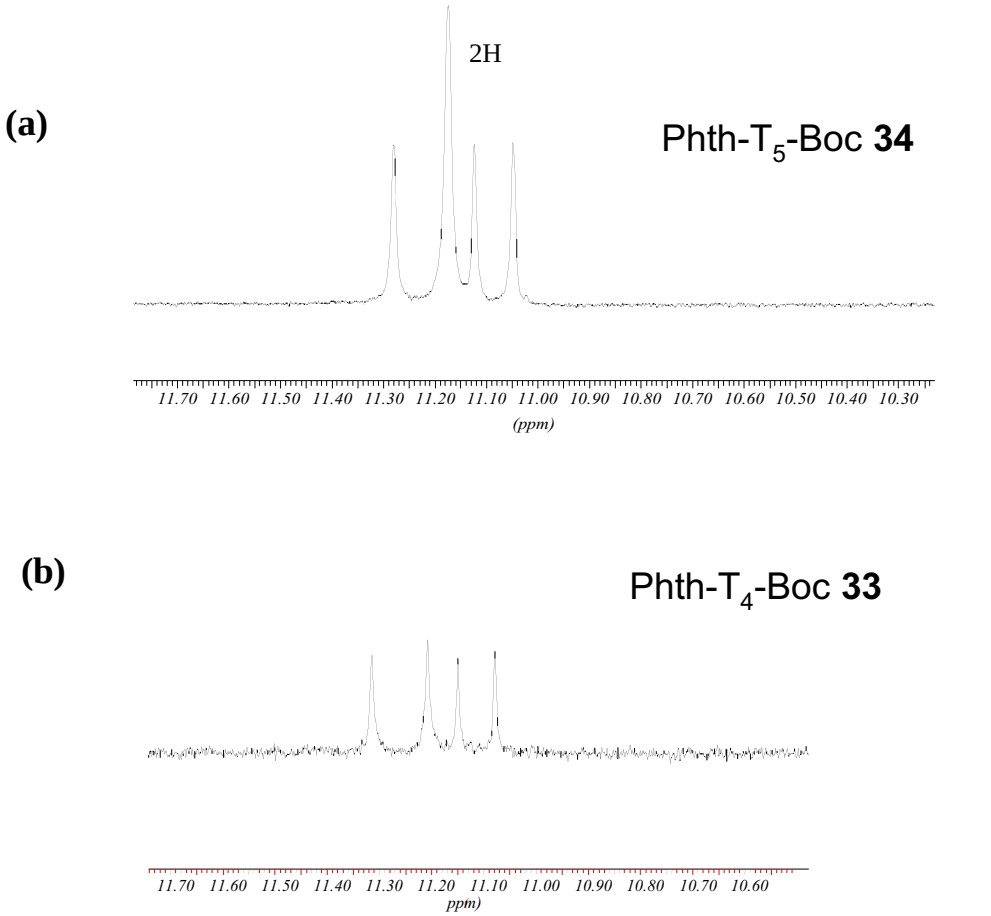

Figure 3

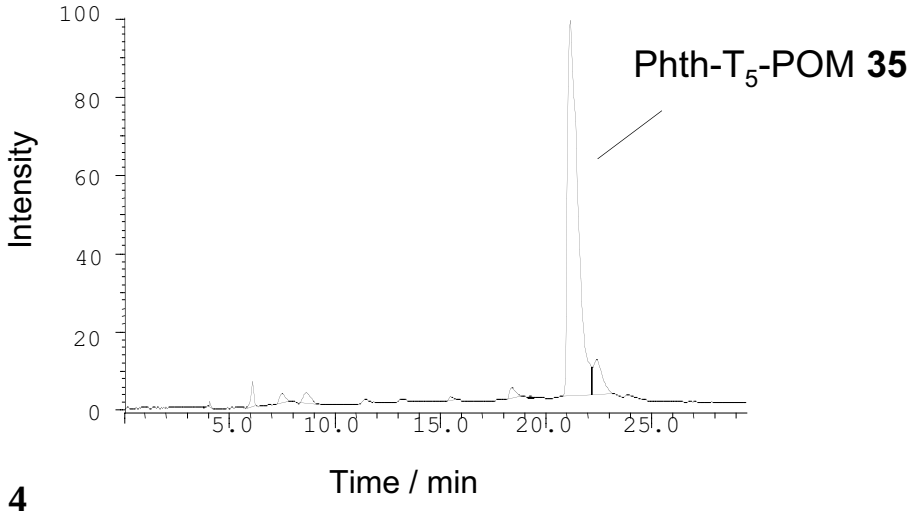

Figure 4

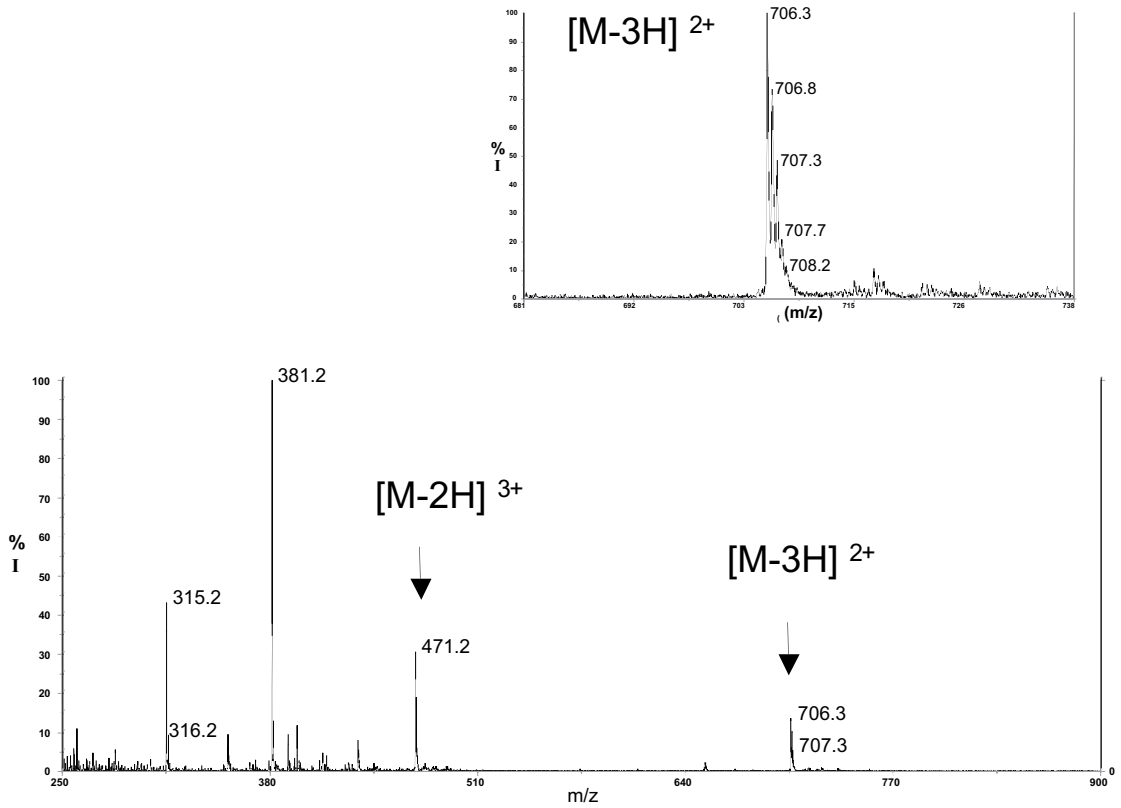
[M-3H] 2+
706.3
706.8
707.3
707.7
708.2
% I
(m/z)
381.2
[M-2H] 3+
[M-3H] 2+
315.2
471.2
316.2
706.3
707.3
% I
m/z

Figure 5.

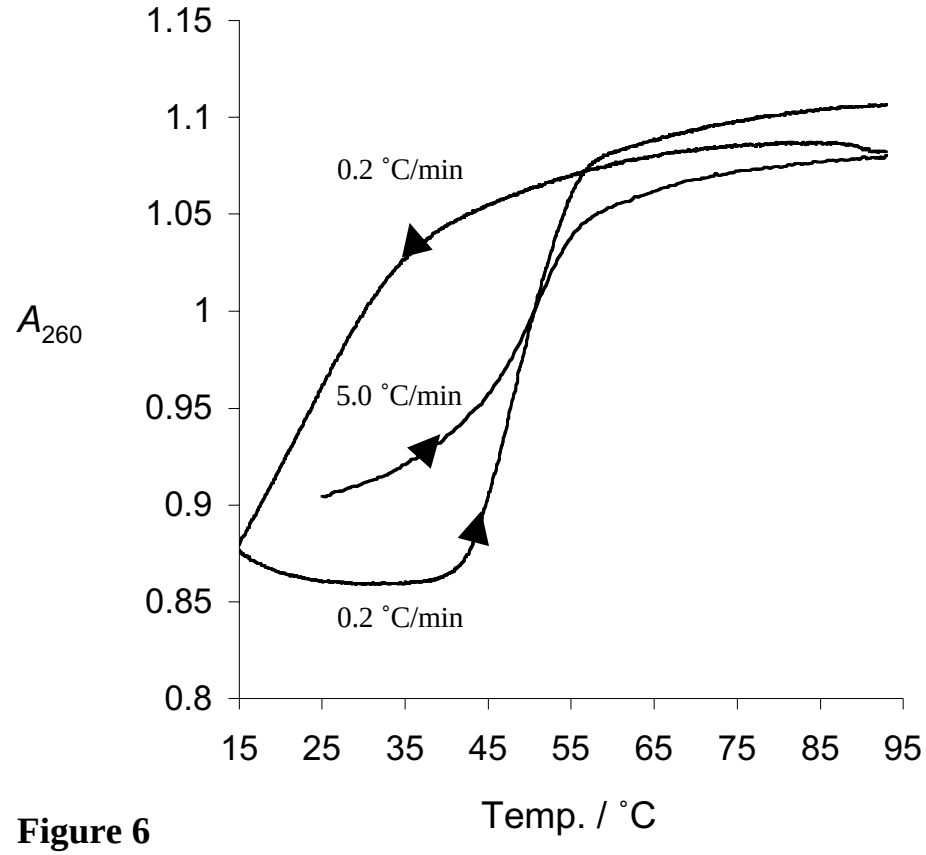

Figure 6

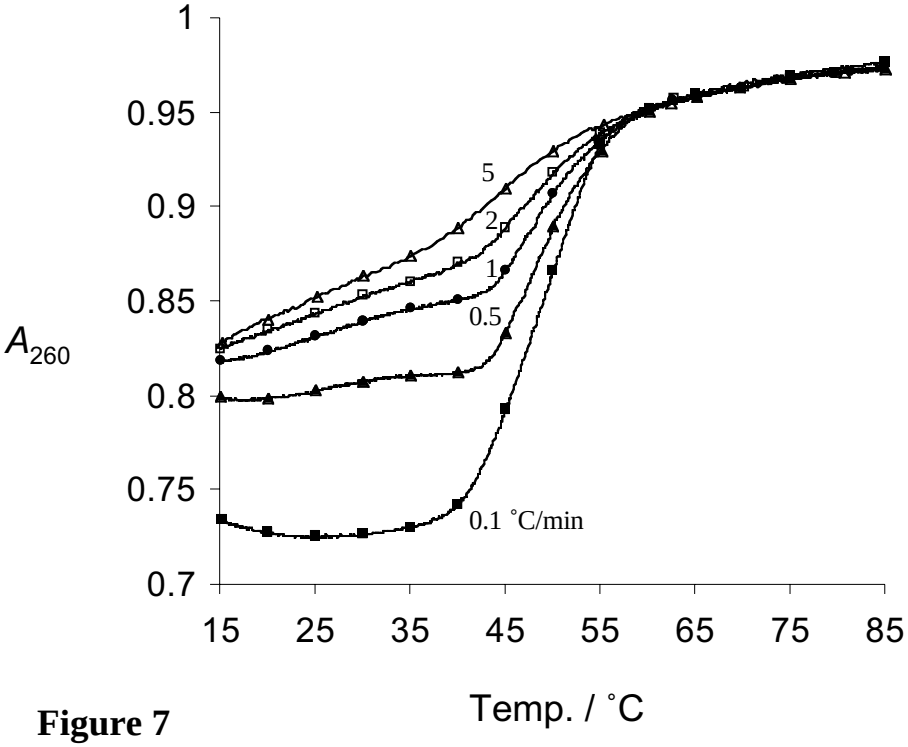

Figure 7

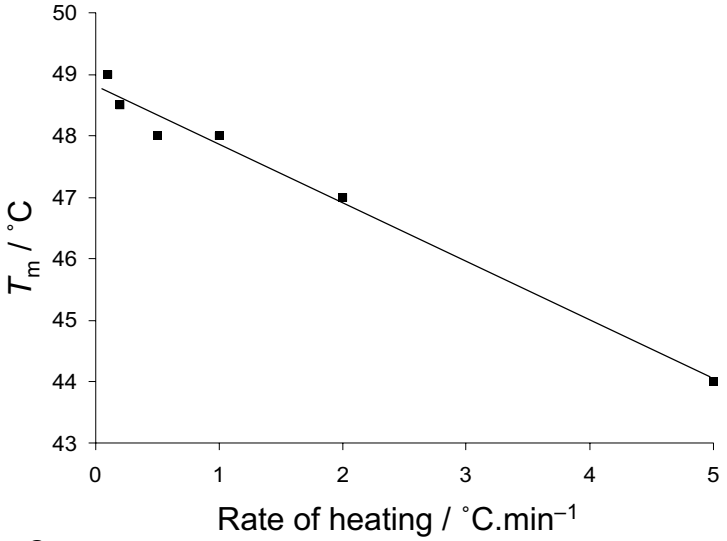

Figure 8

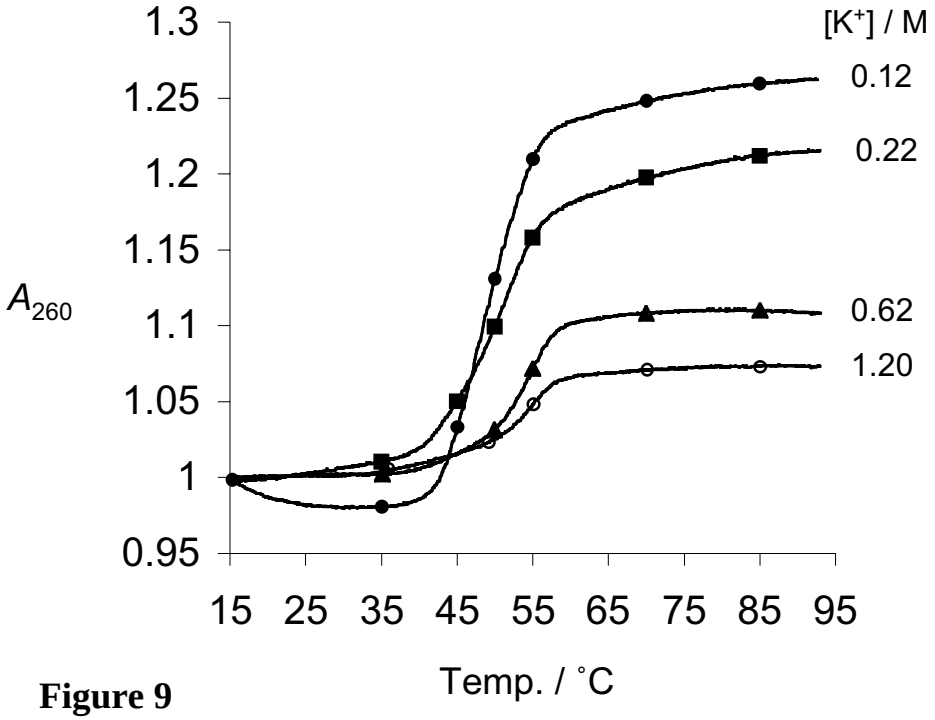

Figure 9

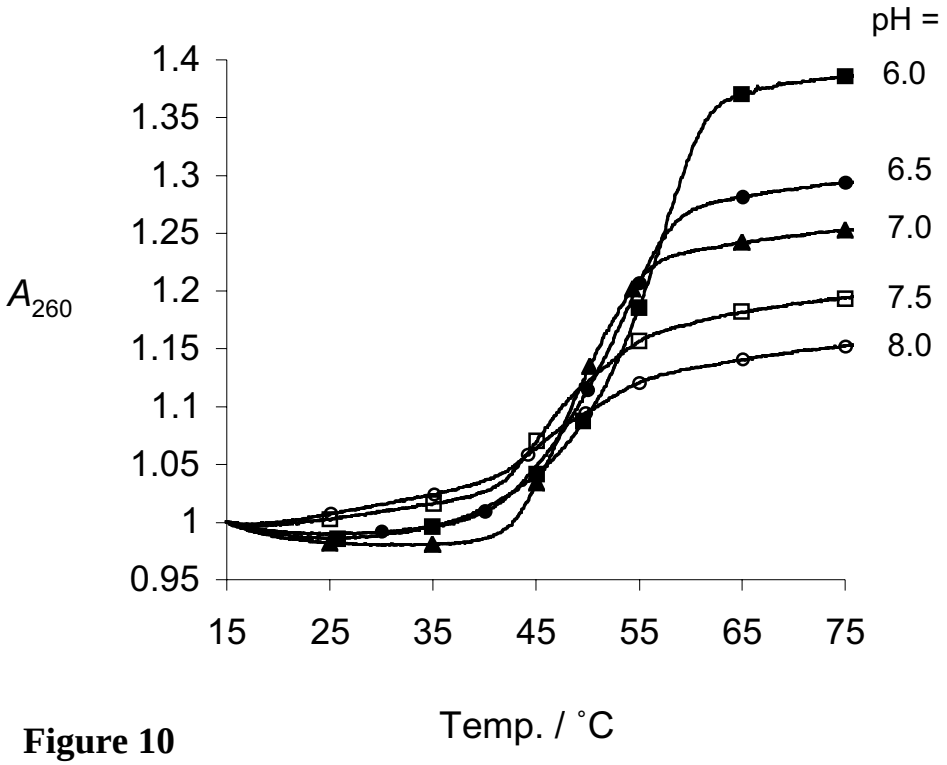

Figure 10

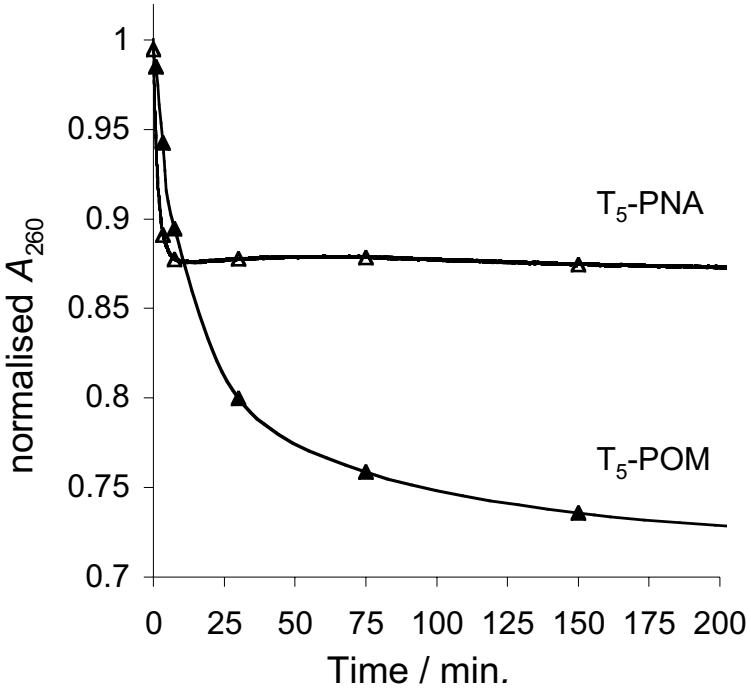

Figure 11

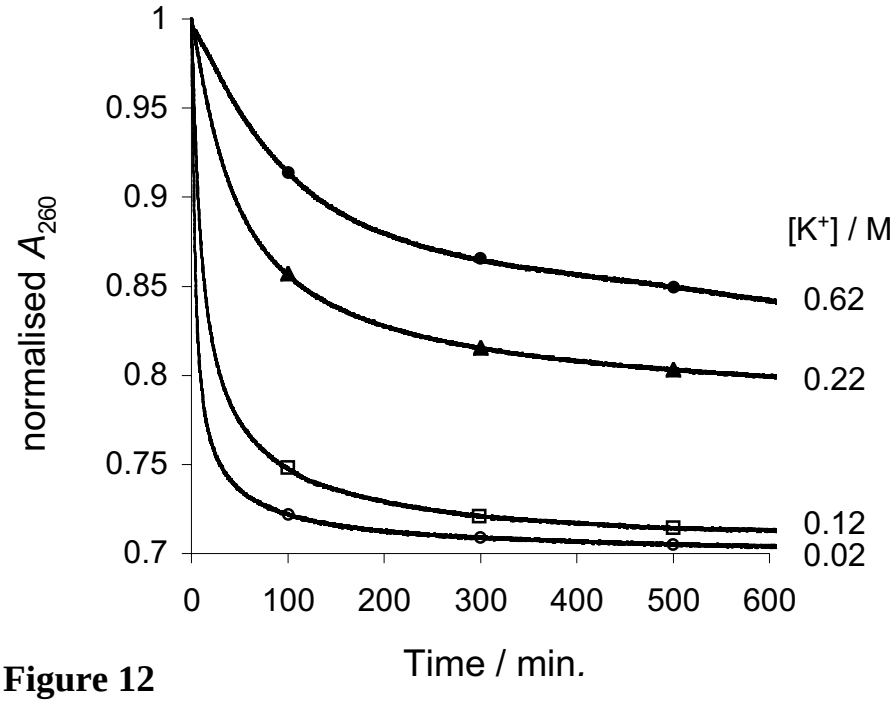

Figure 12

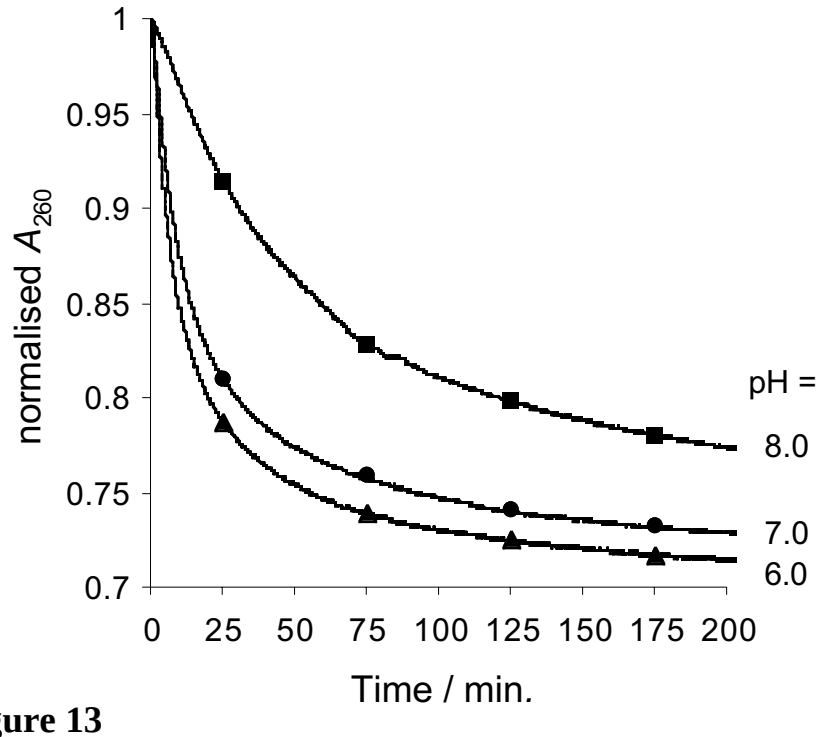

Figure 13

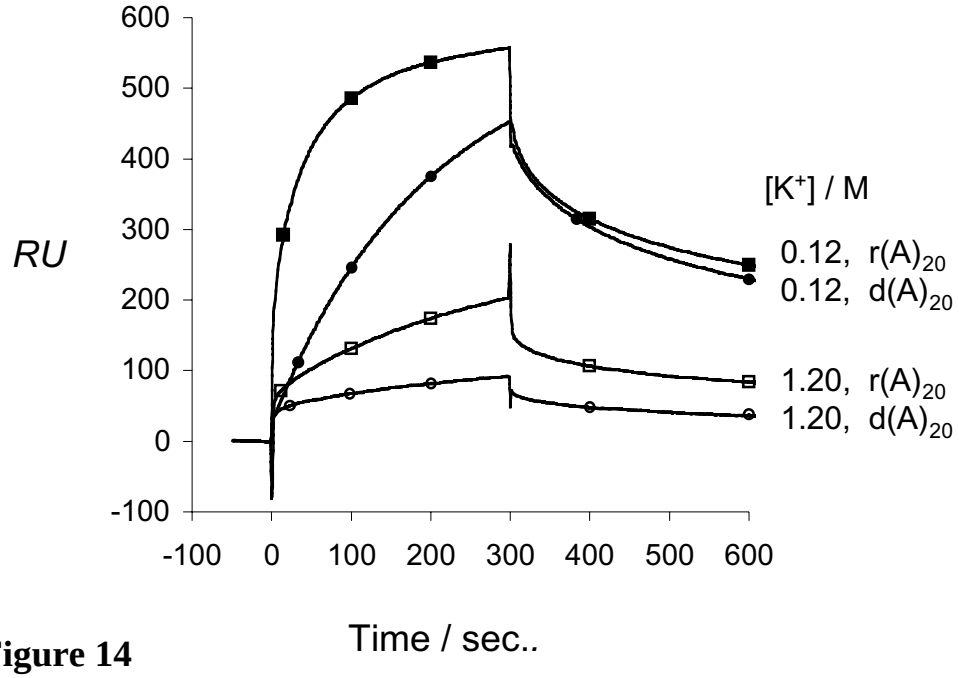

Figure 14

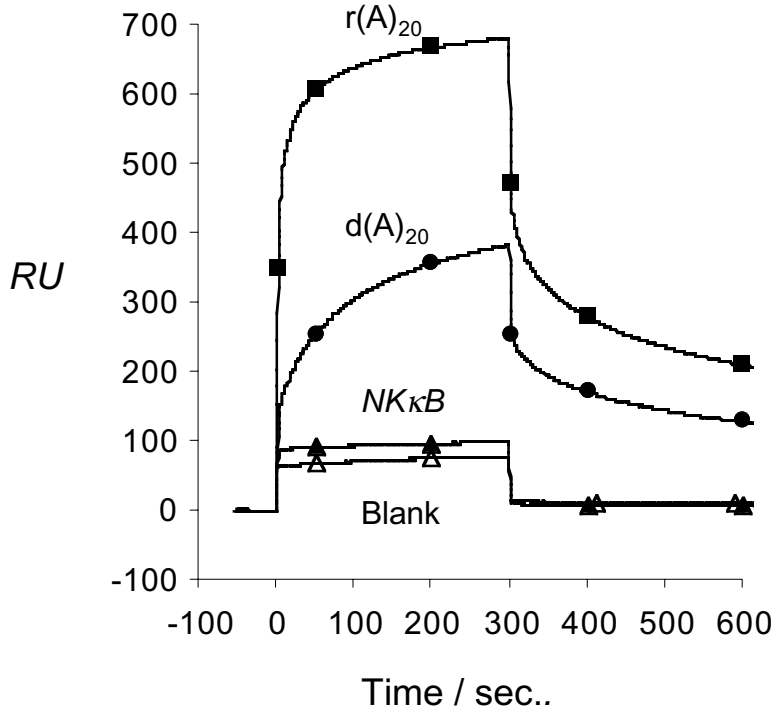

Figure 15

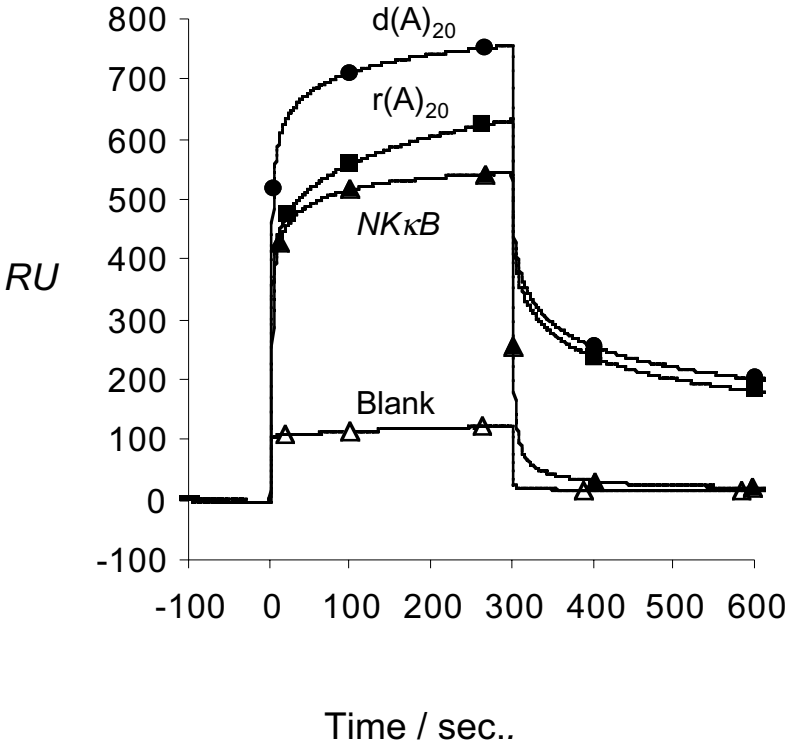
800
700
600
500
400
300
200
100
0
-100
RU
d(A)20
r(A)20
NKκB
Blank
-100
0
100
200
300
400
500
600
Time / sec..

Figure 16